# Modelling and simulation
# of porous immersed boundaries

John M. Stockie *

*Department of Mathematics, Simon Fraser University, 8888 University Drive, Burnaby, BC, V5A 1S6, Canada*

**Abstract**

The immersed boundary method has been used to simulate a wide range of fluid-structure interaction problems from biology and engineering, wherein flexible solid structures deform in response to a surrounding incompressible fluid flow. We generalize the IB method to handle porous membranes by incorporating an additional transmembrane flux that obeys Darcy's law. An approximate analytical solution is derived that clearly illustrates the effect of porosity on the immersed boundary motion. Numerical simulations in two dimensions are used to validate the analytical results and to illustrate the motion of more general porous membrane dynamics.

*Key words:* Immersed boundary method, Porous membrane, Fluid-structure interaction, Volume conservation

## 1 Introduction

The *immersed boundary (IB) method* has proven to be a versatile and robust approach for simulating the interaction of complex, deformable, solid structures with an underlying incompressible fluid flow [23]. The method has been applied extensively to problems arising in bio-fluid dynamics, including blood flow in the heart [24] and arteries [1], biofilms [11], and swimming dynamics of flagellated cells, worms, and other organisms [7]. The IB method has also been utilized for non-biological fluid-structure interaction problems such as suspension flows [27] and parachute dynamics [16].

---
* Tel: +1 778 782 3553. Fax: +1 778 782 4947.
  *Email address:* stockie@math.sfu.ca (John M. Stockie).

The subject of this paper is a class of fluid-structure interaction problems wherein the deformable boundary is also porous, permitting the fluid to flow through it in response to transmural pressure gradients. Such porous immersed boundaries abound in biological systems, including such examples as artery walls [13], brain tissue [26], lipid vesicles and cell membranes [14], and also appear in engineering applications such as ocean wave barriers [5,15] or filtration and separation processes. Most existing numerical methods for simulating flow through porous boundaries assume that the boundary is stationary and does not deform in response to the flow, even though the deformations encountered in actual applications can be substantial; therefore, there is much to be gained by generalizing the IB method to include the effects of porosity.

The only previous attempt to incorporate porosity within the IB framework is a study of parachute dynamics by Kim and Peskin [16] wherein the air vents at the apex of the chute were dealt with by allowing the normal velocity of the canopy to differ from that of the fluid by an amount proportional to the normal component of the boundary force. The IB method has also been used to study flow through granular media at the pore scale by treating the grains making up the medium as immersed boundaries [10], although the grains themselves are rigid and impermeable in these studies. In a study of porous cell membrane transport, Layton [18] generalized the closely-related *immersed interface method* by introducing a porous slip velocity in the normal direction that is driven by differences in both transmural water pressure and solute concentration. However, to date there has been no systematic study of porosity in the context of the IB method.

Our aim in this paper is to extend the IB method to handle porous immersed boundaries in a way that is easily implemented for use in applications. Our treatment is restricted to two dimensions although the extension to 3D is straightforward. We follow Kim and Peskin's approach [16] by incorporating a normal porous slip velocity into the boundary evolution equation. The model equations are presented in Section 2 after which we derive an explicit analytical solution for the special case of a circular membrane subject only to porous leakage. The numerical algorithm is outlined in Section 3, which demonstrates that extending existing IB codes using our approach is straightforward. In Section 4, we draw a connection between errors in volume conservation that are inherent in non-porous IB computations, and the leakage through porous membranes. In particular, these volume errors may be viewed as deriving from an *intrinsic permeability* in the discretized immersed boundary. We investigate the implications of this hypothesis in some detail and are led naturally to a modification of the IB method that corrects for volume errors by introducing an additional porous correction term. Numerical simulations are presented in Section 5 that validate our analytical solution, illustrate more complex porous membrane dynamics, and evaluate our proposed technique for improving volume conservation.

## 2 Mathematical Formulation

We begin by presenting the equations governing the motion of a non-porous boundary immersed in a fluid, following the notation introduced by Peskin [23]. We consider a two-dimensional fluid domain $\Omega$ within which is suspended a single immersed boundary or *membrane* that can be described by a continuous, non-intersecting curve $\Gamma$. The state of the fluid at any position $\vec{x} = (x, y)$ (in s) and time $t$ (s) is described by the velocity $\vec{u}(\vec{x}, t)$ (cm/s) and pressure $p(\vec{x}, t)$ (g/cm s$^2$), which are assumed to obey the incompressible Navier-Stokes equations

$$\rho \left( \vec{u}_t + \vec{u} \cdot \nabla \vec{u} \right) = \mu \Delta \vec{u} - \nabla p + \vec{f}, \tag{1}$$
$$\nabla \cdot \vec{u} = 0. \tag{2}$$

The parameters appearing in the above are the density $\rho$ (g/cm$^3$) and dynamic viscosity $\mu$ (g/cm s), both of which are taken to be constant.

The function $\vec{f}(\vec{x}, t)$ represents the force exerted by the membrane per unit volume of fluid (g/cm$^2$ s$^2$), and is dependent on the current configuration of the membrane. The membrane position is denoted $\vec{X}(s, t) = (X(s, t), Y(s, t))$ where $s$ is a parameterization of the curve in some reference configuration, and so the fluid force may be written as

$$\vec{f}(\vec{x}, t) = \int_\Gamma \vec{F}(s, t)\, \delta(\vec{x} - \vec{X}(s, t))\, ds, \tag{3}$$

where $\delta(\vec{x})$ is the two-dimensional delta function. The function $\vec{F}$ (g/s$^2$), representing the immersed boundary force per unit length, may be written as $\vec{F} = (T\, \vec{\tau})_s$ where $T(s, t)$ is the tension within the membrane and $\vec{\tau}(s, t) = \vec{X}_s / |\vec{X}_s|$ is the unit tangent vector. For the simple case of a linear elastic material that resists both stretching and compression, the membrane tension takes the form $T = \sigma(|\vec{X}_s| - R)$ where the equilibrium state of the membrane is given by $\vec{X}_s = R$ for $R$ some constant, and $\sigma$ (g/cm s$^2$) represents the *spring constant* of the material. With the above definitions, the force density becomes

$$\vec{F} = \sigma \left[ \vec{X}_s \left( 1 - R/|\vec{X}_s| \right) \right]_s, \tag{4}$$

which is a nonlinear function of the IB position $\vec{X}$ except in the special case of a membrane with zero resting where Eq. (4) reduces to $\vec{F} = \sigma \vec{X}_{ss}$.

In order to close the system, an equation governing the membrane motion is required. According to the no-slip condition the membrane must move at the

same velocity as neighbouring fluid particles, which requires that

$$\vec{X}_t = \vec{u}(\vec{X}(s,t),t),$$

which is conveniently written in terms of a delta-function convolution as

$$\vec{X}_t = \int_\Omega \vec{u}(\vec{x},t)\,\delta(\vec{x} - \vec{X}(s,t))\,d\vec{x}. \tag{5}$$

It is important to note the presence of the delta functions in both Eqs. (3) and (5), which leads us naturally to a simple and efficient numerical scheme that will be described in detail in Section 3.

## 2.1  Immersed Boundaries with Porosity

The system of equations (1)–(5) is now generalized to include the effect of porosity in Γ. We follow the approach used by Kim and Peskin [16], who incorporated the effect of air vents in a parachute canopy by introducing a *porous slip velocity* that accounts for air leakage through the vents. The porous flux is directed normal to the chute and is driven by a difference in air pressure from one side to the other – this is a reasonable assumption if the "pores" are directed normally to the chute and have diameter that is small relative to their length. The porous slip velocity can then be expressed as $U_p \vec{n}$ where $\vec{n} = \vec{\tau} \times \vec{e}_3 = (X_s, -Y_s)/|\vec{X}_s|$ is the unit normal vector to Γ, $U_p$ is given by Darcy's law [4] as

$$U_p(s,t) = -\frac{K\,[\![p]\!]}{\mu a}, \tag{6}$$

and $[\![p]\!] = p|_{\Gamma+} - p|_{\Gamma-}$ denotes the jump in pressure. Among the parameters appearing in the above expression, $K$ represents the membrane permeability (cm$^2$) and $a$ is the membrane thickness (cm).

The introduction of a pressure jump in (6) may seem at first to be a significant complication since it introduces a coupling to the momentum equations (1) through the unknown pressure. However, as is demonstrated in [25], Eq. (1) may be integrated to eliminate the delta-function forcing term and obtain instead the following expressions for the jumps in normal and tangential fluid stress across the membrane:

$$-[\![p]\!] + \mu\vec{n} \cdot \left[\!\!\left[\frac{\partial \vec{u}}{\partial n}\right]\!\!\right] = -\frac{\vec{F} \cdot \vec{n}}{|\vec{X}_s|} \qquad \text{and} \qquad \mu\vec{\tau} \cdot \left[\!\!\left[\frac{\partial \vec{u}}{\partial n}\right]\!\!\right] = -\frac{\vec{F} \cdot \vec{\tau}}{|\vec{X}_s|}. \tag{7}$$

The first jump condition may be simplified using the incompressibility condi-

4

tion (2) to obtain

$$[[p]] = \frac{\vec{F} \cdot \vec{n}}{|\vec{X}_s|}, \tag{8}$$

which may be used to rewrite the porous slip velocity in Eq. (6) in terms of the IB force density

$$U_p(s,t) = -\frac{\alpha \vec{F} \cdot \vec{n}}{|\vec{X}_s|}, \tag{9}$$

where the constant $\alpha = \frac{K}{\mu a}$ has units of cm$^2$ s/g. The porous membrane obeys the same governing equations (1)–(4) as in the non-porous case, except that the boundary evolution equation is replaced with

$$\vec{X}_t = -U_p \, \vec{n} + \int_\Omega \vec{u}(\vec{x},t) \, \delta(\vec{x} - \vec{X}(s,t)) \, d\vec{x}, \tag{10}$$

We note that Kim and Peskin's formulation [16] is equivalent to our own if we replace our porous slip parameter $\alpha$ with $\beta\gamma/|\vec{X}_s|$, where $\beta$ is the number density of pores and $\gamma$ is the aerodynamic conductance of the membrane. The main difference between their approach and our own is that we have made explicit use of Darcy's law which permits us to express $\alpha$ in terms of the permeability $K$, a parameter that is easily obtained from experiments. The parameters $\beta$ and $\gamma$, on the other hand, are not commonly available in the porous media literature.

Finally, we close by mentioning the work of Layton [18] who used a similar approach to incorporate porosity into the related immersed interface method, the primary difference being that her method makes explicit use of the stress jump conditions instead of delta function convolutions.

## 2.2   A Simple Analytical Solution

We next derive an explicit analytical solution to the porous IB problem in the case of a circular (radially-symmetric) membrane, centered at the origin in a fluid of infinite extent. To this end, we assume that the unstressed equilibrium state of the membrane is a circle with radius $R_{eq} \geq 0$. Then the membrane configuration at any time $t$ can be written as

$$\vec{X}(s,t) = r(t) \, [\cos s, \sin s], \tag{11}$$

where the parameter $s \in [0, 2\pi]$ corresponds to the polar angle and is measured counter-clockwise around the membrane. The other membrane quantities ap-

pearing in the IB equations may then be expressed as

$$\vec{X}_s = r(t)[-\sin s, \cos s], \qquad \vec{\tau} = [-\sin s, \cos s],$$
$$\left|\vec{X}_s\right| = r(t), \qquad\qquad \vec{n} = [\cos s, \sin s].$$

The membrane resting length in Eq. (4) must be $R = R_{eq}$ in order that the force density at the equilibrium state vanishes; consequently,

$$\vec{F} = \sigma(R_{eq} - r)\,\vec{n}, \tag{12}$$

and the Darcy velocity from Eq. (9) becomes

$$U_p(s, t) = \alpha\sigma\left(1 - \frac{R_{eq}}{r(t)}\right). \tag{13}$$

A simple thought experiment can be used to verify that this velocity behaves as expecte: when $r(t) > R_{eq}$ the membrane is stretched which causes the pressure to be higher inside the membrane and consequently results in the interior fluid leaking outwards (i.e., $U_p > 0$). The opposite is true when $r(t) < R_{eq}$, and when $r(t) = R_{eq}$ the Darcy velocity is identically zero, which implies that there is no porous leakage at the equilibrium state.

If we assume that the fluid velocity is small enough that contributions to the dynamics from the underlying fluid flow are negligible, then the membrane motion is driven primarily by porous effects and Eq. (10) can be approximated by $dr/dt \approx -U_p$. Then, according to Eq. (13), $r(t)$ satisfies the following ordinary differential equation

$$\frac{dr}{dt} = -\alpha\sigma\left(1 - \frac{R_{eq}}{r}\right). \tag{14}$$

When this equation is supplemented by the initial condition $r(0) = R_o$ an explicit analytical solution may be obtained, which we separate into the following two cases.

**Case 1, $R_{eq} = 0$:** For a membrane with a zero resting length, Eq. (14) reduces to $dr/dt = -\alpha\sigma$ which has exact solution

$$r(t) = \begin{cases} R_o - \alpha\sigma t, & \text{if } t < R_o/\alpha\sigma, \\ 0, & \text{otherwise.} \end{cases} \tag{15}$$

The solution is truncated at time $t = R_o/\alpha\sigma$, beyond which the radius is identically zero. This zero-volume steady state is only an idealization since a physical membrane can never actually shrink to a point; nevertheless, it provides an extremely useful test case for computations since it is easy to compute the linear rate of decrease of the membrane radius. The solution profiles corresponding to $\alpha\sigma = 0.016$ cm/s are displayed in Fig. 1 for several

choices of initial radius. If either $\sigma$ or $\alpha$ were increased – corresponding to a stiffer or more porous membrane respectively – then the linear solution profiles would steepen, meaning that the membrane relaxes more rapidly to the equilibrium state.

**Case 2, $R_{eq} > 0$:** In the more general case of a non-zero resting length, the solution to Eq. (14) is

$$r(t) = R_{eq}\Big[1 + W\left(c\exp[-\alpha\sigma t/R_{eq}]\right)\Big],\tag{16}$$

where $c$ is a constant of integration, and $W(x)$ is the Lambert W-function which satisfies $W(x)\,e^{W(x)} = x$ (see [6] for an extensive of review of the properties of $W$). By applying the initial condition, we obtain the constant

$$c = \left(\frac{R_o}{R_{eq}} - 1\right)\exp\left(\frac{R_o}{R_{eq}} - 1\right).\tag{17}$$

We note that the rate of decay depends on the quantity $\alpha\sigma$, just as in the case $R_{eq} = 0$. The time evolution of an initially circular porous membrane having equilibrium radius $R_{eq} = 0.2$ is displayed in Fig. 1 alongside the analytical solution for $R_{eq} = 0$, keeping all other parameter values the same. The primary differences between this and the $R_{eq} = 0$ solution is that the rate of decay to equilibrium is significantly slower, and the radius no longer behaves linearly but rather more in an exponential fashion.

[Fig. 1 about here.]

## 3   Solution Algorithm

The algorithm we describe next is the original IB method proposed by Peskin [22] which is still commonly used especially in bio-fluid applications. The method can be viewed as a mixed Eulerian-Lagrangian approach, wherein the fluid unknowns are approximated on a fixed Cartesian grid and the membrane quantities on a moving set of Lagrangian points. The fluid domain is assumed to be a square $\Omega = [0, L] \times [0, L]$ and is discretized using a uniform $N \times N$ grid with spacing $h = L/N$ in each direction. The time interval $[0, T]$ is divided into $M$ equal sub-intervals of length $k = T/M$. The discrete velocity unknowns may then be written as $\vec{u}_{i,j}^n \approx \vec{u}(x_i, y_j, t_n)$ where $x_i = ih$, $y_j = jh$ for $i, j = 1, 2, \ldots, N$, and $t_n = nk$ for $n = 1, 2, \ldots, M$ (with similar approximations for the pressure $p_{i,j}^n$ and fluid force $\vec{f}_{i,j}^n$). The membrane variables, on the other hand, are discretized at a set of $N_b$ points which move relative to the underlying fluid grid and are parameterized by $s_\ell = \ell h_b$ for $\ell = 1, 2, \ldots, N_b$, where $h_b = 2\pi/N_b$. The discrete IB position and force density are denoted by $\vec{X}_\ell^n$ and $\vec{F}_\ell^n$.

We assume for simplicity that periodic boundary conditions are applied on the sides of the fluid domain, and that the domain is large enough that the neighbouring periodic copies have minimal influence on the membrane motion. We will see shortly that periodicity plays a major role in developing an efficient numerical scheme. We assume further that $\Gamma$ is a closed curve and so the immersed boundary is periodic in $s$.

The discrete approximation of the delta functions appearing in Eqs. (3) and (5) is a fundamental aspect of the IB method. We replace $\delta(\vec{x})$ by a product of one-dimensional discrete delta functions, $\delta(\vec{x}) \approx d_h(x)\,d_h(y)$, where the most common form of $d_h$ employed in computations is

$$d_h(x) = \begin{cases} \frac{1}{4h}\left(1 + \cos\frac{\pi x}{2h}\right), & \text{if } |x| < 2h, \\ 0, & \text{if } |x| \geq 2h. \end{cases}$$

In the context of our Eulerian-Lagrangian scheme, the delta functions act not only to spread the IB forces onto the neighbouring fluid particles in Eq. (3) but also to interpolate fluid velocities onto the IB points in Eq. (5).

Using the definitions introduced above, we are now prepared to outline the algorithm. At the beginning of the $n$th time step, we assume that values of the velocity $\vec{u}_{i,j}^{\,n-1}$ and boundary position $\vec{X}_\ell^{\,n-1}$ are available from the previous step, or else when $n = 1$ from the initial conditions.

1. Calculate the force density $\vec{F}_\ell^{\,n}$ based on $\vec{X}_\ell^{\,n-1}$ using a centered discretization of all derivatives in Eq. (4).
2. Spread the IB force onto nearby fluid points using the following discretization of Eq. (3):

$$\vec{f}_{i,j}^{\,n} = h_b \sum_\ell \vec{F}_\ell^{\,n}\, \delta_h(x_i - X_\ell^{n-1})\, \delta_h(y_j - Y_\ell^{n-1}).$$

3. Integrate the Navier-Stokes equations (1) and (2) using a split-step projection scheme:
   (a) Update the velocity components $\vec{u}_{ij} = (u_{ij}, v_{ij})$ by applying convective, viscous and forcing terms using an alternative direction implicit (ADI) approach and standard second-order centered differences used to approximate all derivatives:

$$\vec{u}_{i,j}^{\,n,0} = \vec{u}_{i,j}^{\,n-1} + \frac{\rho}{k}\,\vec{f}_{i,j}^{\,n},$$

$$\vec{u}_{i,j}^{\,n,1} + \frac{k}{2h}\,u_{i,j}^{n-1}\left(\vec{u}_{i+1,j}^{\,n,1} - \vec{u}_{i-1,j}^{\,n,1}\right) - \frac{\mu k}{\rho h^2}\left(\vec{u}_{i+1,j}^{\,n,1} - 2\vec{u}_{i,j}^{\,n,1} + \vec{u}_{i-1,j}^{\,n,1}\right) = \vec{u}_{i,j}^{\,n,0},$$

$$\vec{u}_{i,j}^{\,n,2} + \frac{k}{2h}\,v_{i,j}^{n-1}\left(\vec{u}_{i,j+1}^{\,n,2} - \vec{u}_{i,j-1}^{\,n,2}\right) - \frac{\mu k}{\rho h^2}\left(\vec{u}_{i,j+1}^{\,n,2} - 2\vec{u}_{i,j}^{\,n,2} + \vec{u}_{i,j-1}^{\,n,2}\right) = \vec{u}_{i,j}^{\,n,1}.$$

   By ordering the velocity unknowns appropriately, the last two equa-

tions take the form of periodic tridiagonal systems and hence can be solved very efficiently.

(b) Project the velocity onto the space of divergence-free vector fields by first solving a Poisson equation for the pressure $p_{i,j}^n$

$$p_{i+2,j}^n + p_{i-2,j}^n + p_{i,j+2}^n + p_{i,j-2}^n - 4p_{i,j}^n = \frac{2\rho h}{k} \left( u_{i+1,j}^{n,2} - u_{i-1,j}^{n,2} + v_{i,j+1}^{n,2} - v_{i,j-1}^{n,2} \right),$$

which is a 5-diagonal linear system that can be inverted efficiently using a Fast Fourier Transform because of the periodic boundary conditions. The velocity is then updated via

$$\vec{u}_{i,j}^n = \vec{u}_{i,j}^{n,2} - \frac{k}{2\rho h} \left( p_{i+1,j}^n - p_{i-1,j}^n, \ p_{i,j+1}^n - p_{i,j-1}^n \right).$$

4. Evolve the boundary points in time using a forward Euler discretization of Eq. (5),

$$\vec{X}_\ell^n = \vec{X}_\ell^{n-1} + \frac{2\alpha k h_b \left( \vec{F}_\ell^n \cdot \vec{n}_\ell^{n-1} \right)}{|\vec{X}_{\ell+1}^{n-1} - \vec{X}_{\ell-1}^{n-1}|} + k h^2 \sum_{i,j} \vec{u}_{i,j}^n \, \delta_h(x_i - X_\ell^{n-1}) \, \delta_h(y_j - Y_\ell^{n-1}).$$

5. Increment $n$ and go to step 1.

The IB method as outlined above has a number of distinct advantages: it is *efficient*, having a computational cost of $O(N^2 \log N)$ owing to the use of the FFT in the projection step; it is *explicit* in the sense that it is a step-by-step approach requiring no iteration; and it is *simple to implement* since no interpolation or complicated difference stencil corrections are needed at the interface like in many other related methods for computing interfacial dynamics (i.e., the delta functions in the IB method handle the interpolation automatically).

On the other hand, the IB method does have some disadvantages, the first being that the centered treatment of convection terms limits the flows that can be handled to low Reynolds number (i.e., $Re = 100$ or less). Since the IB method was originally designed for simulating bio-fluid flow problems where viscous effects typically dominate, this $Re$ restriction is not a serious concern in some applications. The second major disadvantage is that the use of the approximate delta function in combination with a discrete projection limits the accuracy of the method to first order in space. One particular manifestation of this error is a violation of mass conservation which manifests itself as a non-physical slip velocity normal to the membrane – an issue that we treat in more detail in the next section.

These drawbacks stem largely from the specific centered projection scheme described above, although there is nothing to prevent one from using another fluid solver that is more accurate and better suited to high-$Re$ flows. Indeed,

several extensions to the IB method have been proposed in recent years that address the issues mentioned above, including high-order upwind discretizations of the convection terms which allow simulation of convection-dominated flows [17], and use of adaptive mesh refinement near the boundary to obtain second-order accuracy [12].

## 4  Volume Conservation

Before proceeding with the simulations, it is essential to first address the issue of errors in volume conservation in the IB method, since these errors can be large enough to seriously pollute the numerical solution and preclude any meaningful comparisons. The volume loss inherent in the IB method has been recognized for some time, and various approaches have been developed for countering it. Peskin and Printz [25] proposed a modification to the standard centered difference stencils for the gradient, divergence and Laplacian operators which better approximate the divergence-free condition (we will refer to this as the "PP method"). This modification typically reduces the volume error by at least one order of magnitude, but it comes at the expense of approximately doubling the computational cost because of an increase in the difference stencil widths.

Newren [21] observed that when the fluid velocity is interpolated onto IB points using the discrete version of Eq. (5), errors in volume conservation arise because the interpolated velocity does not identically satisfy the divergence-free constraint. He therefore proposed an alternate approach in which the IB velocity is corrected in a post-processing step to ensure that the area contained within the membrane is conserved exactly. The method is simple and efficient, but works only for closed immersed boundaries in two dimensions.

Lee and LeVeque [19] developed a hybrid approach for simulating immersed boundaries, based on a combination of the immersed interface method and the IB method, which uses a higher order correction to the difference stencils for the jump in normal stress across the membrane (i.e., correcting for the pressure jump condition). An entirely different approach called the blob projection method was developed by Cortez and Minion [8] and they include detailed comparisons of their approach with the IB method, as well as extensive discussion of volume conservation.

We propose here an alternate strategy for dealing with volume loss that is inspired by a comment of Peskin and Printz [25], who observed in their computations that *"volume conservation was not exact, and indeed that there was a systematic tendency for a closed, pressurized chamber to lose volume slowly at a rate proportional to the pressure difference across its walls, almost as if the*

*fluid were leaking out through a porous boundary.*" They performed detailed numerical experiments with fluid marker particles to demonstrate that there was no actual leakage of fluid through the immersed boundary. Nonetheless, there is a normal slip velocity which increases with the pressure drop, and so it seems reasonable to suggest that intrinsic volume loss in the IB method can be represented in a manner analogous to flux through a porous membrane flux by introducing an additional normal slip velocity of the form

$$U_v = -\frac{K_v\,[\![p]\!]}{\mu a} = -\frac{K_v(\vec{F}\cdot\vec{n})}{\mu a\,|\vec{X}_s|}, \tag{19}$$

where $K_v$ (units of cm$^2$) is the intrinsic permeability of the discretized immersed boundary. The IB method may then be corrected for volume conservation errors by simply adding a term $U_v\vec{n}$ to the discrete version of Eq. (10). For a porous membrane, this is equivalent to replacing the membrane permeability $K$ with the corrected value $(K - K_v)$.

The membrane thickness $a$ cannot be determined ahead of time since it is actually an *effective thickness* that derives from the smoothing radius of the discrete delta function. Therefore, we choose $a = 4h = 0.0625$ for the purposes of specifying the analytical solution and use the corresponding effective thickness $\widetilde{a} = Ca$ in computations, which is equivalent to replacing the porous slip parameter $\alpha$ with $\widetilde{\alpha} = K/(C\mu a)$. The actual value of the dimensionless parameter $C$ needs to be determined numerically, although we expect that $\widetilde{a}$ will be slightly less than the delta smoothing radius, meaning that $C \lessgtr 1$.

The parameters $K_v$ and $C$ will depend on the discretization (namely, $h$ and/or $h_b$) and so both must be determined computationally for a given problem. We propose the following simple estimation procedure:

1. First perform a simulation with $R_{eq} = 0$ and $K = 0$, and a time interval chosen long enough for the membrane to settle down to its linear rate of decay. The membrane velocity $U_v$ is then approximated from the slope of the $r$ versus $t$ curve, after which Eq. (19) yields an estimate for the intrinsic permeability,

$$K_v \approx -\frac{(\text{slope})\,\mu a\,|\vec{X}_s|}{\vec{F}\cdot\vec{n}}.$$

2. Repeat the simulation from Step 1, taking some positive value of the permeability $K > 0$ and the modified parameter $\widetilde{\alpha} = K/(C\mu a)$. Starting from an initial guess of $C = 1$, adjust $C$ iteratively until the numerical solution coincides with the analytical formula (16).

This is a straightforward procedure that can be easily automated and implemented as an initial *calibration step* in any immersed boundary code.

11

# 5   Numerical Simulations

In this section, we present results from a number of simple test cases to investigate the effectiveness of the porous IB model as well as our new volume correction approach. In order to minimize the effects of intrinsic volume loss and focus instead on the physical porosity, we have chosen to implement the Peskin-Printz (PP) method which ensures that $K_v \ll K$ for the parameters of interest. Their approach is based on modifying the Fourier coefficients of both the pressure solve and the discrete divergence stencil used in the projection step (we refer the reader to [25] for implementation details).

In all of the simulations to follow, we choose a square fluid domain with side length $L = 1$ cm and take fluid parameters $\rho = 1$ g/cm$^3$ and $\mu = 1.0$ g/cm s. Initially, we take $\sigma = 10^5$ g/cm s$^2$ which is typical of other IB simulations for biological flows that have appeared in the literature. The fluid domain is discretized with $N = 64$ points in each direction and the membrane with $N_b = 200$ points.

## 5.1   Circular Membrane: Correcting for Volume Loss

As a first computational test example, we consider a circular membrane with initial radius $R_o = 0.4$ and equilibrium radius $R_{eq} = 0$, for which the analytical solution exhibits a linear decay to equilibrium. This problem is dominated by porous membrane transport since there are no membrane deformations or flow non-uniformities to drive the membrane away from its circular state; hence, this problem represents an ideal scenario for studying porous effects.

In order to determine the volume correction parameters $K_v$ and $C$, we first perform a simulation with $K = 0$ which yields an intrinsic permeability of $K_v = 1.8 \times 10^{-11}$. A second run with $K = 10^{-6}$ (holding all other parameters unchanged) yields the estimate $C = 0.794$, corresponding to a membrane with an effective thickness of $3.17\,h$, which should be compared to the $4h$ support of the delta function. It is worthwhile noting that the volume error arising from $K_v$ will remain small as long as $K_v \ll K$, and so for any given immersed boundary calculation $K_v$ will set a limit on the membrane permeabilities that can reasonably be simulated.

We then perform a series of simulations, holding $K_v$ and $C$ constant while selecting permeabilities from the range $K = [10^{-7}, 10^{-5}]$ in order to determine how robust our proposed method is to changes in $K$. The plots of $r(t)$ given in Fig. 2 indicate that the computed and analytical solutions are nearly indistinguishable from each other, and excellent agreement is obtained over the entire range of $K$ considered. The errors increase as $K$ increases which is to

be expected since a higher permeability will lead to larger porous flux, and when the velocity is large enough convective effects begin to play a significant role. Recall that our analytical solution was derived based on the assumption that convection is negligible, which restricts its validity to small values of $\alpha\sigma$.

[Fig. 2 about here.]

To test the robustness of our volume correction approach to changes in other parameter values, we repeated the previous simulations but took instead a smaller value of the membrane stiffness, $\sigma = 10^4$. In this case, the IB force driving the motion is 10 times smaller and so the solution should exhibit smaller fluid velocities and slower decay rate towards equilibrium. Fig. 3 contains the corresponding error plot for the radius. Keeping in mind that the errors here accumulate over a time interval 10 times longer, we can conclude that the accuracy of our method remains comparable to that of the $\sigma = 10^5$ solution in Fig. 2.

[Fig. 3 about here.]

In order to compare our volume correction approach to other versions of the IB method, we simulate the case of $\sigma = 10^5$ and $K = 10^{-6}$ using the original IB approach and the uncorrected PP method. The error comparison in Fig. 4 indicates that the PP approach is two orders of magnitude more accurate than the original IB method, which is consistent with other studies in the literature [8,25]. When we incorporate our porous correction, the error is reduced by another factor of approximately three.

[Fig. 4 about here.]

Finally, we consider the more realistic situation where $R_{eq} > 0$ and the solution decays to steady state in a nonlinear fashion. Parameters are taken to be $R_{eq} = 0.2$, $\sigma = 10^5$, and permeability is chosen from the range $[10^{-5}, 10^{-7}]$ as before. The results depicted in Fig. 5 again show excellent agreement between the analytical and numerical solutions. The analytical solution (which is included in the plot of radius on the left) is indistinguishable from the computed results, and it is only in the error plot that the discrepancies are visible.

[Fig. 5 about here.]

*5.2 Elliptical Membrane*

Next, we consider a more interesting situation in which the membrane undergoes significant deformations and hence the membrane–fluid coupling plays an important role. To this end, we take the initial membrane to be an ellipse

13

having semi-major and semi-minor axes $r_{max} = 0.4$, $r_{min} = 0.2$, and the unstressed state is a circle of radius $R_{eq} = 0.2$ (this is a slightly modified version of the test problem considered by LeVeque and Li [20]). The membrane oscillates between horizontally- and vertically-elongated states, with the fluid viscosity gradually damping the motion and eventually settling down to a circular steady state (look ahead to Fig. 8 for an illustration of the membrane dynamics). In the non-porous case, the membrane should converge to a circle of radius $\sqrt{r_{min}\, r_{max}} = 0.2828$, while for a porous membrane the steady state circle has radius $R_{eq} = 0.2$.

A comparison of the computed results with and without volume is provided byFig. 6 for $\sigma = 10^5$. The effectiveness of our approach is demonstrated by the plots of average radius and relative error in the area, $|A(t) - A(0)|/A(0)$, where $A(t)$ represents the area enclosed by the membrane and $A(0)$ is the exact (initial) value.

[Fig. 6 about here.]

To investigate the effect of changes in permeability on membrane motion, we repeat the last simulation for a selection of non-zero permeabilities and report the results in Fig. 7. Since the elliptical membrane decays to a circular shape over time, a meaningful comparison is still possible between the numerical solution for the elliptical membrane (in terms of average radius) and our analytical solution (16) for a circular membrane (with $R_o = 0.2828$ and $R_{eq} = 0.2$). The exact solution for each $K$ is included in the plot of radius in Fig. 7 using dashed lines, and once the initial oscillations of the elliptic membrane die out, there is a very close correspondence with the analytical solution.

[Fig. 7 about here.]

The dynamics of the elliptical membrane are more clearly seen in Fig. 8 which depicts the membrane motion throughout the first period of oscillation. The loss of volume owing to porous leakage is also evident from this plot.

[Fig. 8 about here.]

## 6    Conclusions

In this paper, we developed a simple approach for incorporating the effect of membrane porosity in the IB method in two dimensions, which requires the addition of a *porous slip velocity* term to the boundary evolution equation. This modification is easily implemented in an existing IB code, and requires

14

virtually no additional cost since it involves quantities that are already computed. We also derived an explicit, radially-symmetric solution – valid for small values of the permeability $K$ and small flow velocities – which may be used to validate porous IB simulations. The analytical and numerical solutions are compared for a number of membrane geometries and physical parameters, and show very good agreement.

We also investigated the hypothesis that volume conservation errors inherent in the IB method can be attributed to an additional porous flux through the immersed boundary. The rate of volume loss in any given IB computation is dependent on both the discretization and physical parameters, and can be fully captured by introducing two new parameters: an *intrinsic permeability* $(K_v)$ and an *effective membrane thickness* $(Ca)$. We presented a straightforward procedure for estimating $K_v$ and $C$ numerically, and showed that their values remain constant when certain problem parameters are varied. Therefore, our approach has the potential to be a general technique correcting volume errors in the IB method.

Our treatment of volume conservation errors is by no means a comprehensive study and so further work is required to determine the sensitivity of $K_v$ and $C$ to changes in parameters describing the fluid, membrane and discretization. In order to determine how useful our approach is in practice, more extensive simulations are needed that consider not only a wider range of permeabilities relevant to physical applications, but also more general IB configurations.

While our radially symmetric analytical solution is useful in validating computations, analysis of more general 2D membrane configurations would also be of interest. We therefore plan to extend the techniques developed in [28,9] to handle porous immersed boundaries. In future, we also intend to apply our numerical method to the study of specific applications such as the propagation of ocean waves through porous wave barriers, and pulsatile flow of blood through arteries with porous walls. Direct comparisons to other more standard numerical methods for fluid structure interaction such as [3] will also be undertaken, and benchmark problems such as those reported in [2] will be instrumental in demonstrating the practical value of our approach.

## Acknowledgements

# References

[1] K. M. Arthurs, L. C. Moore, C. S. Peskin, E. B. Pitman, and H. E. Layton. Modeling arteriolar flow and mass transport using the immersed boundary method. *J. Comput. Phys.*, 147:402–440, 1998.

[2] K.-J. Bathe and G. A. Ledezma. Benchmark problems for incompressible fluid flows with structural interactions. *Computers & Structures*, 85:628–644, 2007.

[3] K.-J. Bathe and H. Zhang. Finite element developments for general fluid flows with structural interactions. *Int. J. Numer. Meth. Eng.*, 60:213–232, 2004.

[4] J. Bear. *Dynamics of Fluids in Porous Media.* Dover, New York, 1988.

[5] A. T. Chwang. A porous-wavemaker theory. *J. Fluid Mech.*, 132:395–406, 1983.

[6] R. M. Corless, G. H. Gonnet, D. E. G. Hare, D. J. Jeffrey, and D. E. Knuth. On the Lambert W function. *Adv. Comput. Math.*, 5:329–359, 1996.

[7] R. Cortez, L. Fauci, N. Cowen, and R. Dillon. Simulations of swimming organisms: Coupling internal mechanics with external fluid dynamics. *Comput. Sci. & Eng.*, 6(3):38–45, May/June 2004.

[8] R. Cortez and M. Minion. The blob projection method for immersed boundary problems. *J. Comput. Phys.*, 161(2):428–453, 2000.

[9] R. Cortez, C. S. Peskin, J. M. Stockie, and D. A. Varela. Parametric resonance in immersed elastic boundaries. *SIAM J. Appl. Math.*, 65(2):494–520, 2004.

[10] R. Dillon and L. Fauci. Microscale model of bacterial and biofilm dynamics in porous media. *Biotechnol. Bioeng.*, 68(5):536–547, 2000.

[11] R. Dillon, L. J. Fauci, A. L. Fogelson, and D. Gaver III. Modeling biofilm processes using the immersed boundary method. *J. Comput. Phys.*, 129(1):57–73, 1996.

[12] B. E. Griffith, R. D. Hornung, D. M. McQueen, and C. S. Peskin. An adaptive, formally second order accurate version of the immersed boundary method. *J. Comput. Phys.*, 223(1):10–49, 2007.

[13] Z. J. Huang and J. M. Tarbell. Numerical simulation of mass transfer in porous media of blood vessel walls. *Amer. J. Physiol. Heart Circ. Physiol.*, 273(1):464–477, 1997.

[14] J. T. Jenkins. Static equilibrium configurations of a model red blood cell. *J. Math. Biol.*, 4:149–169, 1977.

[15] M. H. Kim and S. T. Kee. Flexible-membrane wave barrier. I: Analytic and numerical solutions. *J. Waterway, Port, Coastal, Ocean Eng.*, 122(1):46–53, 1996.

[16] Y. Kim and C. S. Peskin. 2-D parachute simulation by the immersed boundary method. *SIAM J. Sci. Comput.*, 28(6):2294–2312, 2006.

[17] M. C. Lai and C. S. Peskin. An immersed boundary method with formal second-order accuracy and reduced numerical viscosity. *J. Comput. Phys.*, 160(2):705–719, 2000.

[18] A. T. Layton. Modeling water transport across elastic boundaries using an explicit jump method. *SIAM J. Sci. Comput.*, 28(6):2189–2207, 2006.

[19] L. Lee and R. J. LeVeque. An immersed interface method for incompressible Navier-Stokes equations. *SIAM J. Sci. Comput.*, 25(3):832–856, 2003.

[20] R. J. LeVeque and Z. Li. Immersed interface methods for Stokes flow with elastic boundaries or surface tension. *SIAM J. Sci. Comput.*, 18(3):709–735, 1997.

[21] E. P. Newren. *Enhancing the immersed boundary method: Stability, volume conservation, and implicit solvers*. PhD thesis, University of Utah, Salt Lake City, UT, 2007.

[22] C. S. Peskin. Numerical analysis of blood flow in the heart. *J. Comput. Phys.*, 25:220–252, 1977.

[23] C. S. Peskin. The immersed boundary method. In *Acta Numerica*, volume 11, pages 1–39. Cambridge University Press, 2002.

[24] C. S. Peskin and D. M. McQueen. A three-dimensional computational model for blood flow in the heart. I. Immersed elastic fibers in a viscous incompressible fluid. *J. Comput. Phys.*, 81:372–405, 1989.

[25] C. S. Peskin and B. F. Printz. Improved volume conservation in the computation of flows with immersed elastic boundaries. *J. Comput. Phys.*, 105:33–46, 1993.

[26] S. Sivaloganathan, M. Stastna, G. Tenti, and J. M. Drake. Biomechanics of the brain: A theoretical and numerical study of biot's equations of consolidation theory with deformation-dependent permeability. *Int. J. Nonlin. Mech.*, 40(9):1149–1159, 2005.

[27] J. M. Stockie and S. I. Green. Simulating the motion of pulp fibres using the immersed boundary method. *J. Comput. Phys.*, 147(1):147–165, 1998.

[28] J. M. Stockie and B. T. R. Wetton. Stability analysis for the immersed fiber problem. *SIAM J. Appl. Math.*, 55(6):1577–1591, 1995.
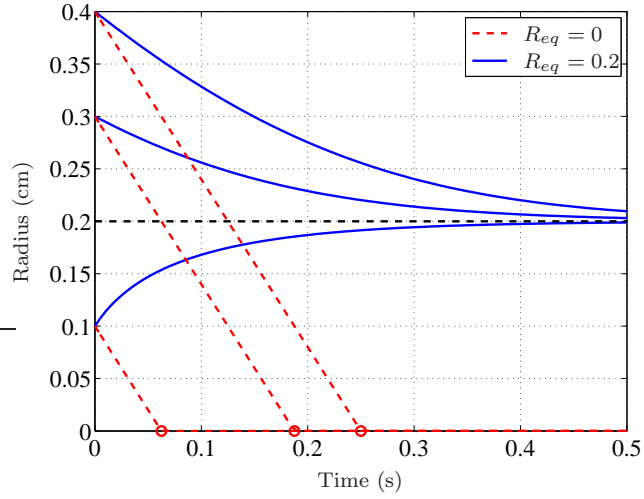
Fig. 1. The analytical solution for a circular membrane is displayed for $\alpha\sigma = 0.016$, equilibrium radii $R_{eq} = 0$ and $0.2$, and initial radii $R_o = 0.1$, $0.3$ and $0.4$. The intercepts $t = R_o/\alpha\sigma$ for the $R_{eq} = 0$ solution are depicted on the $t$–axis using open circles.
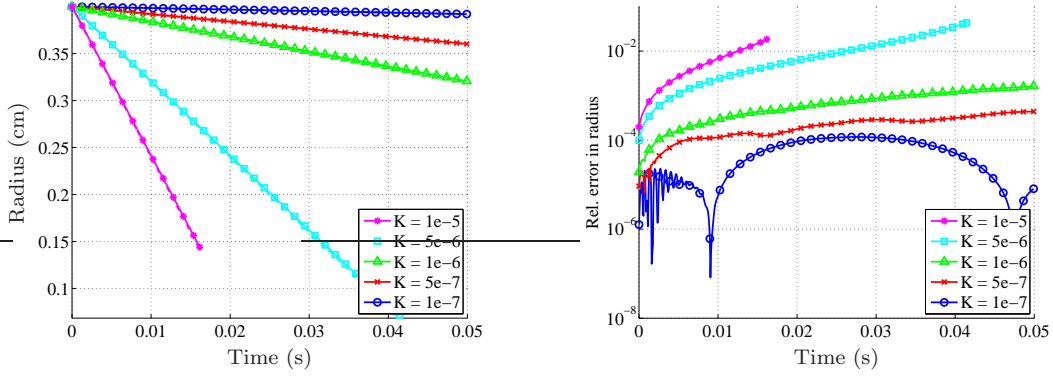
Fig. 2. Circular membrane with $\sigma = 10^5$ and $R_{eq} = 0$ and various values of $K$. Left: The analytical solution (dashed lines) is plotted alongside the computed solution (solid lines), from which the results are indistinguishable. Right: The relative error in the radius is plotted for each value of $K$. The simulations for the two largest values of $K$ are terminated early because of a numerical instability arising from excessive clustering of IB points as the membrane shrinks.
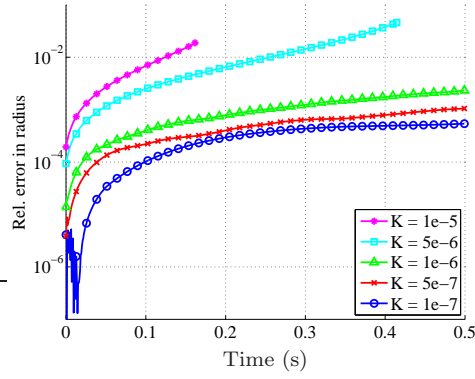
Fig. 3. Circular membrane with $\sigma = 10^4$ and $R_{eq} = 0$. The relative error in the membrane radius is plotted for the same values of $K$ as in Fig. 2.

20
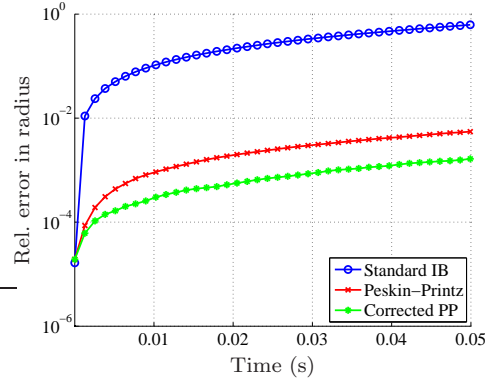
Fig. 4. Plots of solution error for the circular membrane with $\sigma = 10^5$, $R_{eq} = 0$, and $K = 10^{-6}$, using three different methods for correcting volume loss: the standard IB method, and the PP volume-conserving stencil with $K_v = 0$ and $1.8 \times 10^{-11}$.
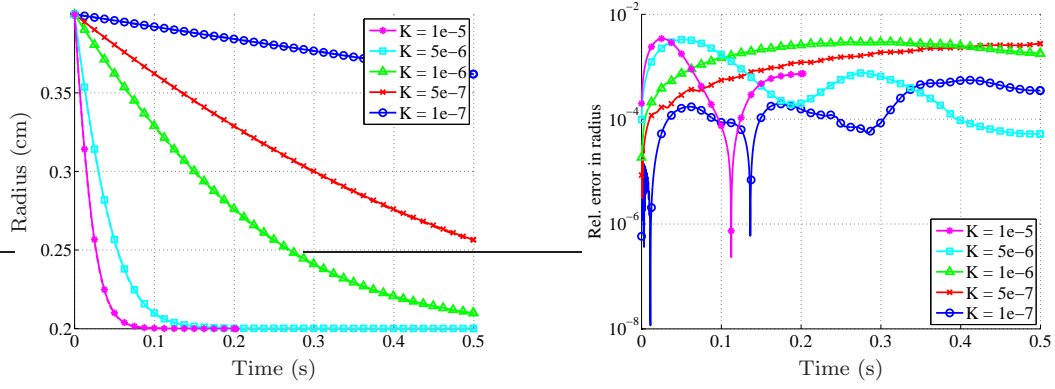
Fig. 5. Plots of the radius (left) and error (right) for the circular membrane with $\sigma = 10^5$, $R_{eq} = 0.2$, and various values of $K$.
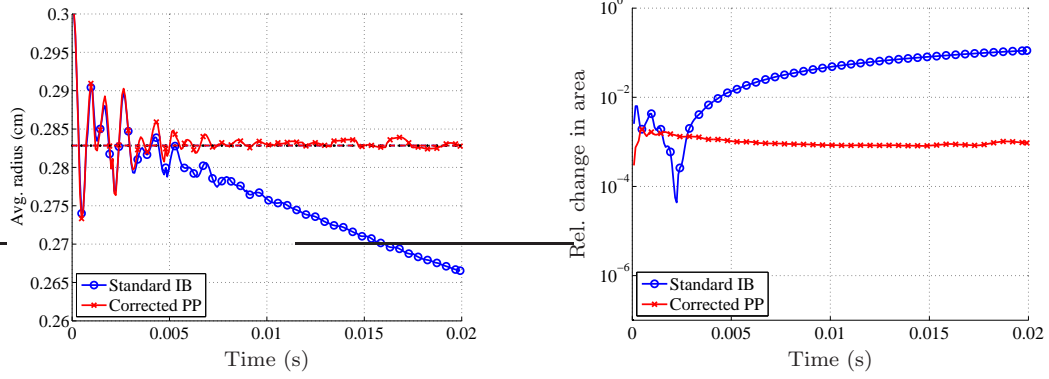
Fig. 6. Elliptical membrane with $\sigma = 10^5$ and $K = 0$, simulated using the standard IB method and our volume correction approach. Left: Average radius, with the circular steady state $r = 0.2828$ denoted by a dotted black line. Right: Relative error in the area.
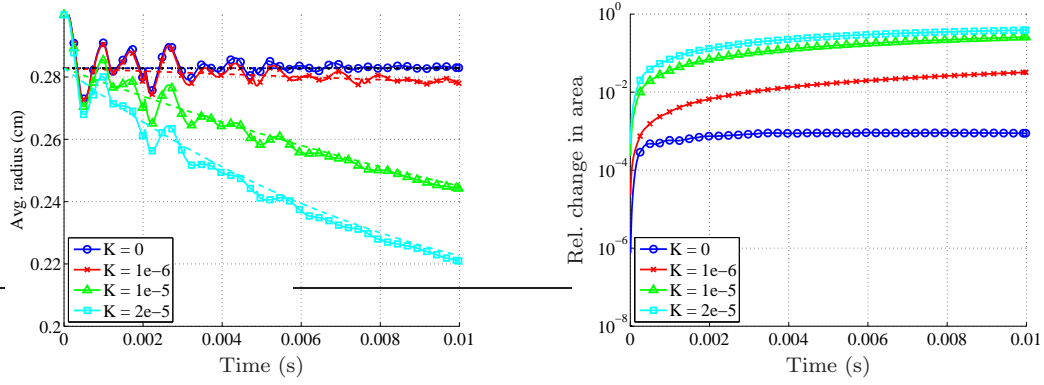
Fig. 7. Elliptical membrane with $\sigma = 10^5$ and various values of the permeability. Left: Average radius, with the corresponding circular exact solutions plotted using dashed lines. Right: Relative change in radius, $|A - A(0)|/A(0)$.
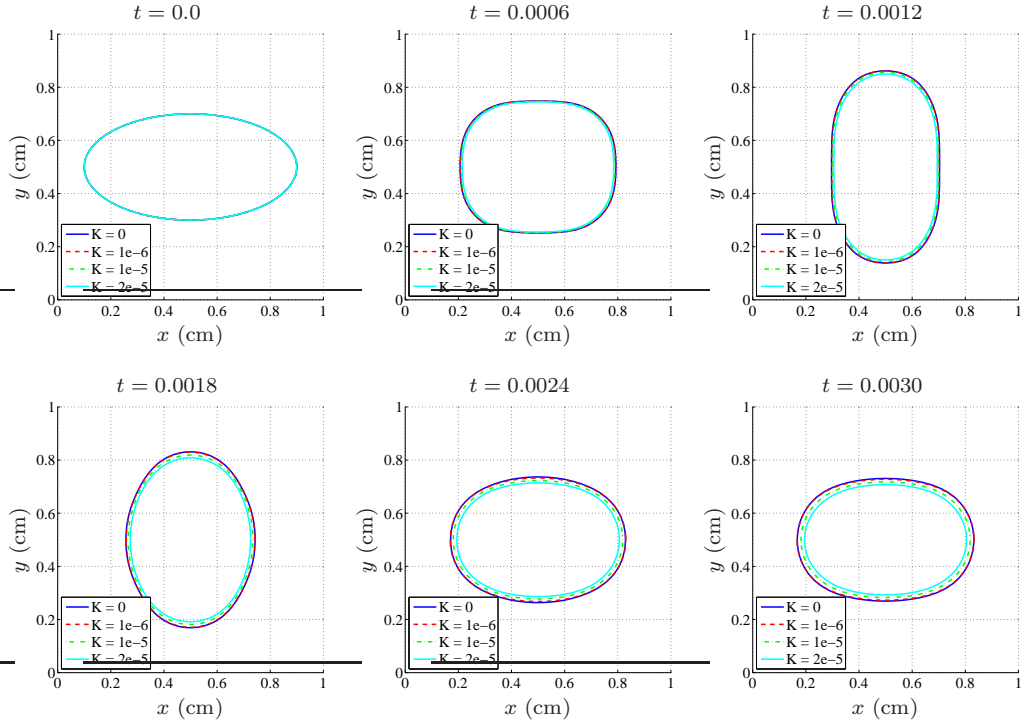
Fig. 8. Time evolution of an elliptical membrane with $\sigma = 10^5$ and various values of $K$.